Resolution below the point spread function for diffuse optical imaging using fluorescence lifetime multiplexing

William L. Rice, Steven Hou, and Anand T. N. Kumar*

Athinoula A. Martinos Center for Biomedical Imaging, Department of Radiology, Massachusetts General Hospital, Harvard Medical School, Charlestown, Massachusetts 02129, USA
*Corresponding author: ankumar@nmr.mgh.harvard.edu

We show that asymptotic lifetime-based fluorescence tomography can localize multiple-lifetime targets separated well below the diffuse point spread function of a turbid medium. This is made possible due to a complete diagonalization of the time domain forward problem in the asymptotic limit. We also show that continuous wave or direct time gate approaches to fluorescence tomography are unable to achieve this separation, indicating the unique advantage of a decay-amplitude-based approach for tomographic lifetime multiplexing with time domain data.   © 2013 Optical Society of America

OCIS codes: (170.3880) Medical and biological imaging; (170.6920) Time-resolved imaging; (170.6960) Tomography.
http://dx.doi.org/10.1364/OL.38.002038

Fluorescence tomography is commonly performed using continuous wave (CW) [1] or frequency domain (FD) excitation and detection. CW systems, although low cost and easy to implement, have limited flexibility for multiplexing and provide a resolution (center-to-center distance) of 4–5 mm for small animal imaging [1]. Detection of multiple probes with CW techniques requires fluorophores with significant spectral separation [2], and is further limited by the relatively narrow range of the near infra-red spectrum that is useful for tomographic applications. While FD systems allow lifetime detection [3], resolving multiple lifetimes reliably requires the use of multiple frequencies [4]. Time-resolved techniques, using ultrashort pulsed excitation and gated detection, have recently gained prominence and provide several advantages, including lifetime multiplexing [5,6] and early photon gating [7,8], allowing for higher resolution. In addition to the use of spectrally similar fluorophores, time-resolved imaging enables the separation of fluorophore signals from complex decays arising from tissue autofluorescence [9].

Previously, we have shown that an asymptotic time domain (ATD) approach, based on a multi-exponential analysis of the decay portion of the temporal response, provides an accurate localization of fluorescence yield distribution and is superior to CW [10], FD [11], and direct time domain (DTD) [12] methods in terms of separability of yield distributions for multiple-lifetime fluorophores. The strength of the ATD approach is in its ability to completely separate the 3D yield distributions of each lifetime from a mixture of lifetimes present in the imaging medium. This feature implies a unique advantage of ATD: whereas CW-based reconstructions are unable to resolve targets separated by distances smaller than the intrinsic point spread function (PSF) [13], the peaks of each ATD unmixed yield distribution can accurately resolve the localization of targets separated well below the width of the PSF (although individually these distributions are governed by the same PSF). In this Letter, we use phantom measurements to demonstrate that this unique

feature of the ATD approach enables the spatial localization of tubes separated by 1.4 mm, with a 30% difference in fluorescence lifetime between the tubes. This resolution represents a nearly threefold improvement over that achieved with CW alone [1]. We also show that a brute force approach to invert the time domain (TD) data directly using multiple gates [14] is unable to achieve this separation.

Assuming that the fluorophores under study have lifetimes τ_n that are longer than the intrinsic diffusion time scales (a condition widely satisfied for biological tissue [12]), the TD fluorescence signal asymptotically approaches a multi-exponential sum, with decay amplitudes a_n linearly related to the yield distributions $\eta_n(\mathbf{r})$ of the particular lifetime τ_n as $a_n(\mathbf{r}_s, \mathbf{r}_d) = \int_\Omega d^3 r \bar{W}_n(\mathbf{r}_s, \mathbf{r}_d, \mathbf{r}) \eta_n(\mathbf{r})$, where $\mathbf{r}_s$, $\mathbf{r}_d$, and $\mathbf{r}$ denote, respectively, the locations of the source, the detector on the surface, and a point inside the imaging medium with volume Ω. $\bar{W}_n(\mathbf{r}_s, \mathbf{r}_d, \mathbf{r}) = \bar{G}_n^x(\mathbf{r}_s, \mathbf{r}) \bar{G}_n^m(\mathbf{r}, \mathbf{r}_d)$ is the CW Born sensitivity function with $\bar{G}_n^{x,m}$ as the Green functions evaluated at a background absorption reduced by $(v\tau_n)^{-1}$ [12], and v is the speed of light in the medium. Considering a two-lifetime case, we can express the ATD approach in the following matrix form:

$$\begin{pmatrix} a_1^j \\ a_2^j \end{pmatrix} = \begin{pmatrix} \bar{W}_1^j & \mathbf{0} \\ \mathbf{0} & \bar{W}_2^j \end{pmatrix} \begin{pmatrix} \eta_1(\mathbf{r}) \\ \eta_2(\mathbf{r}) \end{pmatrix}, \qquad (1)$$

where j indicates the measurement index ($\mathbf{r}_s$, $\mathbf{r}_d$ pair). Thus, the ATD results in a complete diagonalization of the diffuse fluorescence forward problem with respect to the yield distributions $\eta_n(\mathbf{r})$. This should be contrasted with CW, FD, and DTD approaches, where each measurement is related to all the η_n values [10,11]. Coupled with the fact that the decay amplitudes a_n can be directly obtained from linear fits to the asymptotic portion of the raw fluorescence data, Eq. (1) offers a powerful approach to obtain separate reconstructions for each fluorophore in a mixture based on their distinct lifetimes [11,12].

In order to illustrate the ability of ATD to resolve targets within the limits of the diffuse PSF [which still limits the individual distributions for CW and each $\eta_n(\mathbf{r})$], we constructed three phantoms consisting of cell culture dishes [88 mm diameter, 17 mm in height, with two parallel tubes (0.965 mm outer diameter, 0.58 mm inner diameter) spanning the length of the dish, at a height of 8 mm, and a center-to-center separation of 5.6, 2, or 1.4 mm (see Fig. 1)]. The tubes were filled with 3, 3′-diethylthiatricarbocyanine iodide (DTTC) dye at a concentration of either 7.4 μM in 100% ethanol ($\tau_L = 1.27$ ns) or 9.2 μM in 66% ethanol, 33% H_2O ($\tau_S = 0.88$ ns). These concentrations were selected to achieve similar CW fluorescence yield for the two dyes in the absence of scattering medium, since the focus of the present work is the recovery of the tube locations without the influence of intensity variations. The fluorescence lifetime of each DTTC solution was measured directly in the absense of scattering medium. All phantoms were filled with 99 mL of 1% intralipid with 4.34 μg/mL nigrosin, resulting in a reduced scattering coefficient of 10 cm^{-1} and an absorption coefficient of 0.1 cm^{-1} at 770 nm. The phantoms were imaged in a transmission geometry with the time-resolved system described previously [10]. Fluorescence was excited at 770 nm with a Ti:sapphire laser and detected with an 800 nm long pass filter coupled to an intensified CCD camera (PicostarHR, LAVision, Gmbh; 500 ps gate width, 600 V gain, 150 ps steps, 2×2 hardware binning). Complete domain data were recorded for multiple source positions (Fig. 1) arranged across the dye-filled tubes in three rows, spaced at 6.8 mm, and separated by either 1.8 mm (5.6 mm tube separation) or 1.4 mm (2 and 1.4 mm tube separation). For tomography, detectors were selected as points on the phantom surface directly above each source.

For each source, amplitude maps were recovered across the entire CCD image using a linear fit to a bi-exponential model with fixed lifetimes of 1.27 and 0.88 ns. Importantly, the linear approach is also feasible with *in vivo* applications, where the lifetimes can be determined *a priori* using separate measurements with each dye present in the animal [5]. In Fig. 2, the resulting amplitude maps are displayed for each phantom, with the long and short lifetime amplitudes represented as red and green components of a single RGB image matrix. A cross-sectional profile perpendicular to the long axis of the
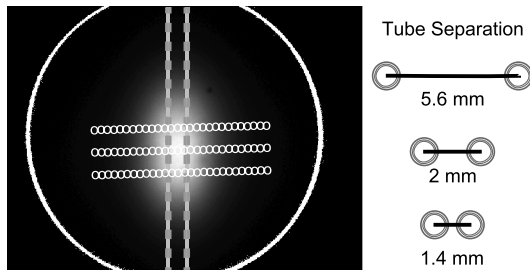
Fig. 1. Dish phantom filled with intralipid and nigrosin solution to a depth of 1.7 cm, shown with the tubes. Parallel dye-filled tubes have a center-to-center separation of 5.6 (shown), 2, or 1.4 mm. Also shown are source and detector positions (o) overlaid on top of the total CW fluorescence intensity distribution for all sources.
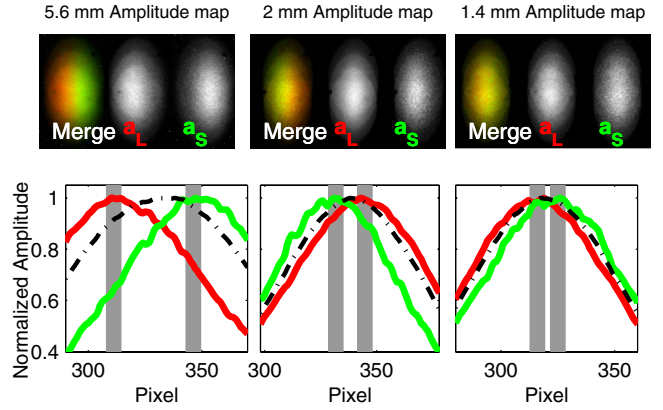
Fig. 2. Fluorescence lifetime amplitude maps and line profiles for each phantom measurement. The peak of the amplitude distribution for the long (a_L, $\tau_L = 1.27$ ns, red) component and the short (a_S, $\tau_S = 0.88$ ns, green) component reveals the correct position of the corresponding dye-filled tube (indicated by gray bars). The individual tube positions are not evident from the CW (integrated TD) fluorescence (black dash–dotted line).

tubes shows that the peak of the amplitudes accurately matches the corresponding true tube positions. However, a cross section of the total fluorescence intensity (CW) is unable to resolve the position of the tubes, even at a separation of 5.6 mm. Here, the power of the asymptotic approach to decompose a single fluorescence dataset into separate amplitude maps is evident, and illustrates that even in planar images, lifetime contrast enables the detection of targets embedded in a turbid medium, separated by as little as 1.4 mm. However, tomography is necessary to accurately localize the fluorophores for more complex medium geometries and to recover the *in vivo* concentrations.

To recover the 3D yield distribution of each dye [$\eta_L(\mathbf{r})$ and $\eta_S(\mathbf{r})$], we employed the ATD approach as described in Eq. (1) [10]. The Green functions $\tilde{G}_n^{x,m}$ were generated from Monte–Carlo simulations of light propagation performed with the MCX software package: 200 million photons launched through a cylindrical geometry ($176 \times 176 \times 36$, 0.125 mm^3 voxels) with optical properties matching that of the liquid phantom. Reconstructions were then performed with Tikhonov regularization in conjunction with singular value decomposition (SVD) analysis by solving the underdetermined forward problem $Y = WX$ in MATLAB (The Mathworks, Inc) as $X = L^{-1}VS(S^2 + \alpha\lambda I)^{-1}U^T Y$, where L is a spatially variant regularization vector [10], $\alpha = \max\{\text{diag}(W^T W)\}$, λ is the Tikhonov regularization parameter, and U, S, V are the SVD matrices of WL^{-1}. In Fig. 3 we display a single x–z slice from the CW, DTD, and ATD fluorescence yield reconstructions (thresholded at 90% of maximum) as well as normalized line profiles for each case. Both the DTD and the CW approaches can resolve tubes with center-to-center separations of 5.6 mm but fail to resolve the 2 or 1.4 mm cases for any value of the regularization parameter λ. Both the 2 and 1.4 mm separations are well below the width of the typical PSF ($\approx$4–5 mm) for a 2 cm thick diffusive slab [13] (the intrinsic PSF is also roughly represented by the distributions for each η_n and the CW in Fig. 3). The shift of the CW reconstructions toward the
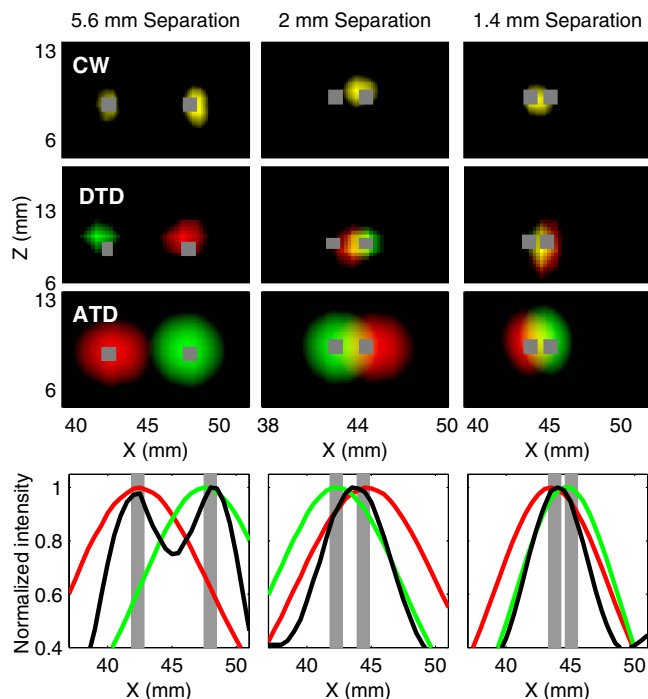
Fig. 3.   3D fluorescence reconstructions using CW, DTD, and ATD approaches for three tube separations. Top three rows: x–z projections of the reconstructions along a central slice through the phantom. The ATD and DTD yield distributions are shown for the long (η_L) and short (η_S) lifetimes as the red and green components of an RGB image. Bottom row: corresponding normalized profiles of CW and ATD yield reconstructions along a line at a depth of 8.5 mm.

long-lifetime tube for the 2 and 1.4 mm cases could be attributed to the slightly larger net yield of the 1.27 ns dye compared to the 0.88 ns dye.

Although the individual ATD distributions (η_S and η_L) are limited by the intrinsic PSF, the peaks of the distributions for each lifetime (red and green lines in Fig. 3) accurately represent the true tube locations for all three cases for a range of λ. The recovered tube separations for the ATD reconstructions were 5.5 (± 0.88), 2.17 (± 0.19), and 1.2 mm (± 0.06 mm) at $\lambda = 1$. It is noteworthy that the DTD reconstructions used up to 18 time gates spanning the entire fluorescence decay and were thus computationally several orders more cumbersome than the ATD approach. The failure of the DTD approach to localize short separations can be attributed to the cross talk between multiple lifetimes as discussed previously [12]. However, note that the distributions for the DTD and CW are narrower than that for ATD, due to the better signal quality in these data sets. This allows the use of smaller regularizations. These methods are thus more

appropriate when no lifetime contrast is present in the medium. A detailed comparison study between the DTD and ATD approaches will be presented in future work.

In summary, we have demonstrated that the ATD approach for TD fluorescence optical tomography enables the separation of targets located well below the intrinsic PSF for diffuse optics. An essential requirement for this approach is a lifetime contrast between the targets, and we have shown that a 30% lifetime variation allows the separation of targets as close as 1.4 mm. While these results do not represent a lower limit on either the required lifetime contrast or the achievable spatial separation, they illustrate a clear advantage of the ATD approach over CW and a brute force direct time gate approach [12,14]. In this Letter, we have mainly focused on the ability of ATD to recover the spatial localization without any emphasis on contrast resolution [13]. Future work will explore the contrast resolution as well as the spatial resolution performance of ATD as a function of lifetime separation and its application for *in vivo* imaging.

References

1. E. E. Graves, J. Ripoll, R. Weissleder, and V. Ntziachristos, Med. Phys. **30**, 901 (2003).
2. X. Gao, Y. Cui, R. M. Levenson, L. W. K. Chung, and S. Nie, Nat. Biotechnol. **22**, 969 (2004).
3. A. Godavarty, E. M. Sevick-Muraca, and M. J. Eppstein, Med. Phys. **32**, 992 (2005).
4. J. R. Lakowicz, *Principles of Fluorescence Spectroscopy*, 3rd ed. (Springer, 2006), pp. 157–199.
5. S. B. Raymond, D. A. Boas, B. J. Bacskai, and A. T. N. Kumar, J. Biomed. Opt. **15**, 046011 (2010).
6. R. E. Nothdurft, S. V. Patwardhan, W. Akers, Y. Ye, S. Achilefu, and J. P. Culver, J. Biomed. Opt. **14**, 024004 (2009).
7. Z. Li and M. Niedre, Biomed. Opt. Express **2** 665 (2011).
8. F. Leblond, H. Dehghani, D. Kepshire, and B. W. Pogue, J. Opt. Soc. Am. A **26**, 1444 (2009).
9. A. T. N. Kumar, E. Chung, S. B. Raymond, J. A. J. M. van de Water, K. Shah, D. Fukumura, R. K. Jain, B. J. Bacskai, and D. A. Boas, Opt. Lett. **34**, 2066 (2009).
10. A. T. N. Kumar, S. B. Raymond, A. K. Dunn, B. J. Bacskai, and D. A. Boas, IEEE Trans. Med. Imaging **27**, 1152 (2008).
11. A. T. N. Kumar, S. B. Raymond, B. J. Bacskai, and D. A. Boas, Opt. Lett. **33**, 470 (2008).
12. A. T. N. Kumar, S. B. Raymond, G. Boverman, D. A. Boas, and B. J. Bacskai, Opt. Express **14**, 12255 (2006).
13. B. W. Pogue, S. C. Davis, X. Song, B. A. Brooksby, H. Dehghani, and K. D. Paulsen, J. Biomed. Opt. **11**, 33001 (2006).
14. J. Chen, V. Venugopal, and X. Intes, Biomed. Opt. Express **2**, 871 (2011).